Electronic supplementary information (ESI)

Direct synthesis of acetic acid from carbon dioxide and methane over Cu-modulated BEA, MFI, MOR and TON zeolites: A density functional theory study

Sen Wang,[a] Shujia Guo,[a,b] Yaoya Luo,[a,b] Zhangfeng Qin,*,[a] Yanyan Chen,[a] Mei Dong,[a] Junfen Li,[a] Weibin Fan,*,[a] Jianguo Wang*,[a,b]

[a] *State Key Laboratory of Coal Conversion, Institute of Coal Chemistry, Chinese Academy of Sciences, P.O. Box 165, Taiyuan, Shanxi 030001, PR China*

[b] *University of the Chinese Academy of Sciences, Beijing 100049, PR China*

* *Corresponding authors. Tel.: +86-351-4046092; Fax: +86-351-4041153. E-mail address: qzhf@sxicc.ac.cn (Z. Qin); fanwb@sxicc.ac.cn (W. Fan); iccjgw@sxicc.ac.cn (J. Wang)*

As the Electronic supplementary information (ESI) of the manuscript "*Direct synthesis of acetic acid from carbon dioxide and methane over Cu-modulated BEA, MFI, MOR and TON zeolites: A density functional theory study*", following materials are provided:

Calculated unit cell parameters for the BEA, MFI, MOR and TON zeolites; calculated adsorption energy of CH_4 on various model systems; substitution energy and occupation probability of Al substituting for Si in the BEA, MFI, MOR and TON zeolites; projected density of states (PDOS) for the transition state of CH_4 dissociation and the detailed optimized transition states of various reaction steps for the direct conversion of carbon dioxide and methane into acetic acid.

Description of the optimized transition states for the direct conversion of carbon dioxide and methane to acetic acid over Cu-modulated MFI, MOR and TON zeolites, which were not discussed in detail in the main text:

1. CH_4 adsorption

MFI zeolite. As shown in Figs. S6–S8, ESI, when CH_4 molecule is adsorbed on the $[Cu]^{2+}$ (Figs. S6a), $[CuOCu]^{2+}$ (Figs. S7a) and $[Cu_3(\mu\text{-}O)_3]^{2+}$ (Figs. S8a) sites, the C–H bond of CH_4 extends to 1.100–1.126 Å, whereas the bond lengths of Cu–H and O–H contract to 1.905–2.871 Å and 2.811–3.162 Å, respectively.

MOR zeolite. The geometry of CH_4 adsorption on the Cu-modulated MOR zeolites is shown in Figs. S9–S11, ESI. After being adsorbed, the C–H bond of CH_4 extends to 1.105–1.112 Å, with the bond distances of 2.112–2.507 Å for Cu–H and 2.595–2.782 Å for O–H.

TON zeolite. As depicted in Figs. S12–S14, ESI, after the adsorption of CH_4, the C–H bond of CH_4 on $[Cu]^{2+}$ (Figs. S12a), $[CuOCu]^{2+}$ (Figs. S13a) and $[Cu_3(\mu\text{-}O)_3]^{2+}$ (Figs. S14a) is lengthened to 1.124, 1.100 and 1.101 Å, respectively, whereas the Cu–H bond lengths on three sites are 2.595, 2.901 and 2.951 Å and the O–H bond lengths on three sites are 2.995, 2.411 and 3.012 Å, respectively.

2. CH_4 dissociation

MFI zeolite. The dissociation of CH_4 on the Cu-modulated MFI zeolites is illustrated in Figs. S6–S8, ESI. The C–H bond of CH_4 in the transition states is lengthened to 1.801, 1.713 and 1.311 Å on $[Cu]^{2+}$ (Fig. S6b), $[CuOCu]^{2+}$ (Fig. S7b) and $[Cu_3(\mu\text{-}O)_3]^{2+}$ (Fig. S8b), respectively, whereas the O–H bond on three sites is shortened to 1.126, 1.022 and 1.252 Å, respectively.

MOR zeolite. Figs. S9–S11, ESI depict the dissociation of CH_4 on the Cu-modulated MOR zeolite. The C–H bond in the transition states extends to 1.341–1.463 Å, whereas the O–H bond is shortened to 1.114−1.234 Å.

TON zeolite. The optimized transition states of CH_4 dissociation on the Cu-modulated TON zeolites are shown in Figs. S12–S14, ESI. The bond lengths of C–H in the transition states on $[Cu]^{2+}$ (Fig. S12b), $[CuOCu]^{2+}$ (Fig. S13b) and $[Cu_3(\mu\text{-}O)_3]^{2+}$ (Fig. S14b) are 1.995, 1.347 and 1.484 Å, respectively, whereas the bond lengths of H–O on three sites are 1.028, 1.227 and 1.096 Å, respectively.

3. C–C coupling between the methyl group and CO_2

MFI zeolite. For the C–C coupling over Cu-modulated MFI zeolites, as depicted in Figs. S6–S8, ESI, the distance of C–C bond between –CH_3 and CO_2 in the transition states is shortened to 1.808–1.878 Å, whereas the length of Cu–C bond between the Cu site and –CH_3 group is extended to 2.143–2.240 Å. CO_2 molecule shows an obvious bent configuration with the O–C–O bond angle of 139.5–142.1°.

MOR zeolite. As shown in Figs. S9–S11, ESI, for the insertion of CO_2 into the Cu–CH_3 complex, the C–C bond lengths in the transition states on the $[Cu]^{2+}$ (Fig. S9c), $[CuOCu]^{2+}$ (Fig. S10c) and $[Cu_3(\mu\text{-}O)_3]^{2+}$ (Fig. S11c) sites are 1.767, 1.724 and 1.872 Å, respectively, whilst the Cu–C bond lengths on three sites are 2.208, 2.639 and 2.568 Å and the O–C–O bond angles of CO_2 bend from 180° to 142.7–144.9°.

TON zeolite. The optimized transition states for the C–C coupling step over Cu-modulated TON zeolites are shown in Figs. S12–S14, ESI. The length of C–C bond between –CH_3 and CO_2 is shortened to 1.895–1.995 Å, whereas the length of Cu–C bond between Cu and –CH_3 is extended to 1.950–2.241 Å and the O–C–O bond angle of CO_2 is in the range of 141.9–152.9°.

4. Protonation of acetate intermediate

MFI zeolite. The protonation of CH_3COO^- intermediate over the Cu-modulated MFI zeolites is depicted in Figs. S6–S8, ESI. The lengths of two O–H bonds for the transition states on the $[Cu]^{2+}$ (Fig. S6d), $[CuOCu]^{2+}$ (Fig. S7d) and $[Cu_3(\mu\text{-}O)_3]^{2+}$ (Fig. S8d) sites are 1.466 and 1.156 Å, 1.396 and 1.210 Å, and 1.412 and 1.118 Å, respectively.

MOR zeolite. For the protonation of CH_3COO^- intermediate over Cu-modulated MOR zeolite, as shown in Figs. S9–S11, ESI, the H–O bond length of the Brønsted acid site is lengthened to 1.114–1.156 Å, whereas the H–O bond length between the Brønsted acid site and CH_3COO^- is shortened to 1.399–1.526 Å.

TON zeolite. Figs. S12–S14, ESI show the optimized transition states for the protonation of CH_3COO^- intermediate over Cu-modulated TON zeolites. The H–O bond length of the Brønsted acid site is lengthened to 1.019–1.055 Å, whereas the H–O bond length between the Brønsted acid site and CH_3COO^- is shortened to 1.559–1.640 Å.

Table S1. Calculated unit cell parameters for the BEA, MFI, MOR and TON model systems and corresponding experimental values

Zeolite system	*a* (Å)	*b* (Å)	*c* (Å)
BEA-this work	12.193	12.207	25.928
BEA-Exp [1]	12.661	12.661	26.406
MOR-this work	17.772	19.651	14.602
MOR-Exp [2]	18.250	20.530	15.080
MFI-this work	19.421	19.349	13.031
MFI-Exp [3]	20.070	19.920	13.420
TON-this work	13.428	16.982	14.640
TON-Exp [4]	13.859	17.420	15.114

Table S2. Calculated adsorption energy of CH_4 on various Cu-modulated BEA, MFI, MOR and TON zeolites with ($E_{\text{ads-d}}$, kJ mol^{-1}) and without (E_{ads}, kJ mol^{-1}) considering the dispersion correction

Zeolite	$[Cu]^{2+}$		$[CuOCu]^{2+}$		$[Cu_3(\mu\text{-}O)_3]^{2+}$	
	$E_{\text{ads-d}}$	E_{ads}	$E_{\text{ads-d}}$	E_{ads}	$E_{\text{ads-d}}$	E_{ads}
BEA	−108	−87	−26	9	−38	−15
MFI	−89	−64	−49	−30	−40	−6
MOR	−77	−44	−18	−20	−27	−1
TON	−98	−77	−56	−13	−85	−37

Table S3. Calculated activation energy of the CH_4 dissociation (TS1), C–C coupling (TS2) and protonation of acetate (TS3) steps for the direct conversion of carbon dioxide and methane to acetic acid over various Cu-modulated BEA, MFI, MOR and TON zeolites with ($E_{\text{a-d}}$, kJ mol^{-1}) and without (E_{a}, kJ mol^{-1}) considering the dispersion correction

Zeolite	$E_{\text{a-d}}$ (kJ mol^{-1})			E_a (kJ mol^{-1})		
	$[Cu]^{2+}$	$[CuOCu]^{2+}$	$[Cu_3(\mu\text{-}O)_3]^{2+}$	$[Cu]^{2+}$	$[CuOCu]^{2+}$	$[Cu_3(\mu\text{-}O)_3]^{2+}$
BEA						
TS1	135	62	86	158	55	85
TS2	190	173	201	179	167	197
TS3	178	65	65	179	71	78
MFI						
TS1	194	63	106	217	64	112
TS2	224	142	218	220	150	246
TS3	103	87	52	88	77	60
MOR						
TS1	137	54	36	153	52	37
TS2	172	184	160	174	185	148
TS3	109	96	81	99	88	72
TON						
TS1	191	67	82	217	57	68
TS2	155	168	144	217	173	142
TS3	59	126	47	52	125	56

Table S4. Calculated Bader charge of CO_2 and $–CH_3$ group for the reactants and products of the C–C coupling step over BEA and MFI carrying $[CuOCu]^{2+}$, and MOR and TON bearing $[Cu_3(\mu\text{-}O)_3]^{2+}$

Zeolite	Reactant		Product	
	CO_2	$–CH_3$	CO_2	$–CH_3$
$[CuOCu]^{2+}$-BEA	+2.01 |e|	–0.26 |e|	+1.68 |e|	–0.15 |e|
$[CuOCu]^{2+}$-MFI	+2.12 |e|	–0.32 |e|	+1.69 |e|	–0.13 |e|
$[Cu_3(\mu\text{-}O)_3]^{2+}$-MOR	+2.08 |e|	–0.28 |e|	+1.50 |e|	–0.17 |e|
$[Cu_3(\mu\text{-}O)_3]^{2+}$-TON	+2.11 |e|	–0.28 |e|	+1.71 |e|	–0.19 |e|

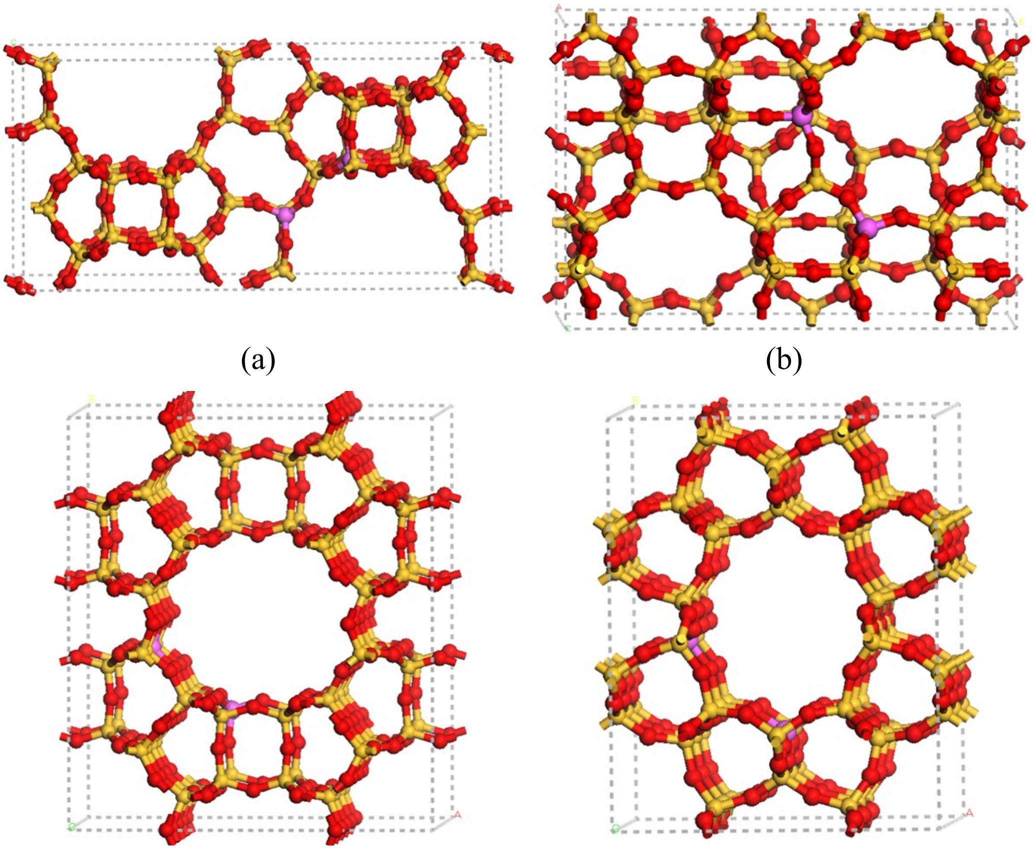

(a) (b)

(c) (d)

Fig. S1. Periodic zeolite models of BEA with two Al atoms substituted for Si atoms at the T4–T4 sites of intersection cavity (a), MFI with two Al atoms substituted for Si atoms at the T12–T2 sites of intersection cavity (b), MOR with two Al atoms substituted for Si atoms at the T1–T4 sites of intersection cavity, and TON with two Al atoms substituted for Si atoms at the T1–T3 sites of intersection cavity (d).

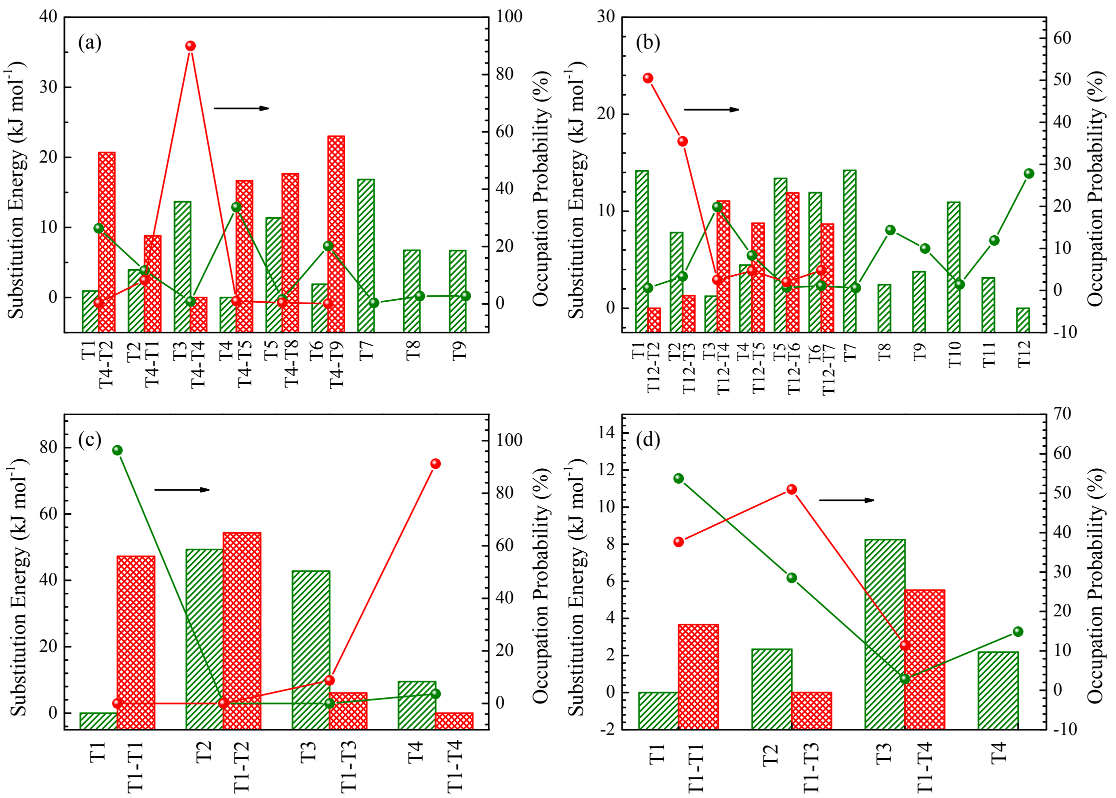

Fig. S2. Substitution energy and occupation probability for the mono-substitution (green) of one Al atom for one Si atom and bi-substitution (red) of two Al atoms for two Si atoms in the BEA (a), MFI (b), MOR (c) and TON (d) zeolites.

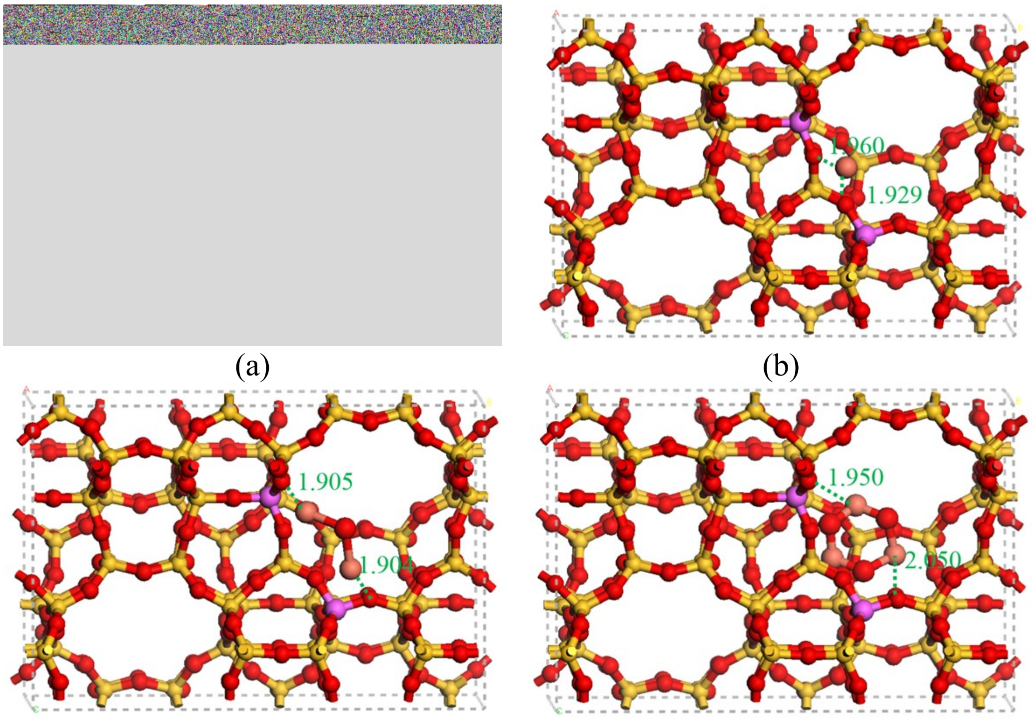

(a) (b)

(c) (d)

Fig. S3. Periodic MFI zeolite model with two Al atoms substituted for Si atoms at the T12–T2 sites of intersection cavity (a) and subsequent Cu-modulated MFI where negative charge resulted from Al substitution was compensated by mononuclear $[Cu]^{2+}$ (b), binuclear $[CuOCu]^{2+}$ (c), and trinuclear $[Cu_3(\mu\text{-}O)_3]^{2+}$ (d). Atomic coloring: Si, yellow; O, red; Al, pink; and Cu, brown. The units of bond distance and bond angle are Å and degree, respectively.

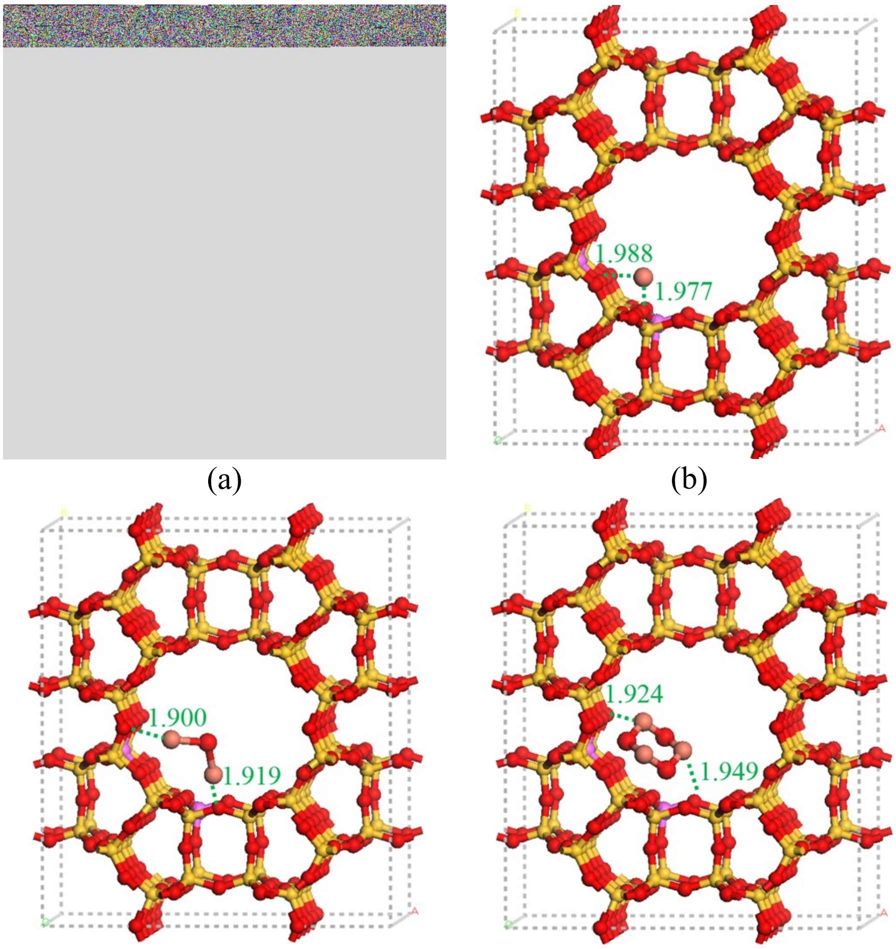

(a) (b)

(c) (d)

Fig. S4. Periodic MOR zeolite model with two Al atoms substituted for Si atoms at the T1–T4 sites of intersection cavity (a) and subsequent Cu-modulated MOR where negative charge resulted from Al substitution was compensated by mononuclear $[Cu]^{2+}$ (b), binuclear $[CuOCu]^{2+}$ (c), and trinuclear $[Cu_3(\mu\text{-}O)_3]^{2+}$ (d). Atomic coloring: Si, yellow; O, red; Al, pink; and Cu, brown. The units of bond distance and bond angle are Å and degree, respectively.

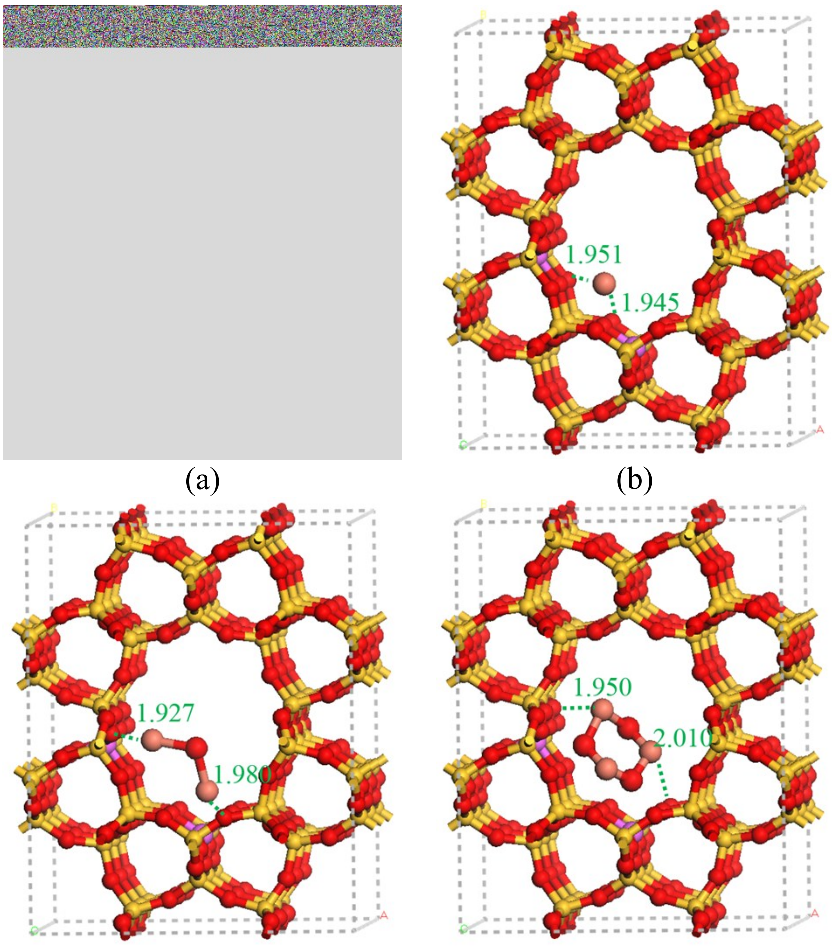

(a) (b)

(c) (d)

Fig. S5. Periodic TON zeolite model with two Al atoms substituted for Si atoms at the T1–T3 sites of intersection cavity (a) and subsequent Cu-modulated TON where negative charge resulted from Al substitution was compensated by mononuclear $[Cu]^{2+}$ (b), binuclear $[CuOCu]^{2+}$ (c), and trinuclear $[Cu_3(\mu\text{-}O)_3]^{2+}$ (d). Atomic coloring: Si, yellow; O, red; Al, pink; and Cu, brown. The units of bond distance and bond angle are Å and degree, respectively.

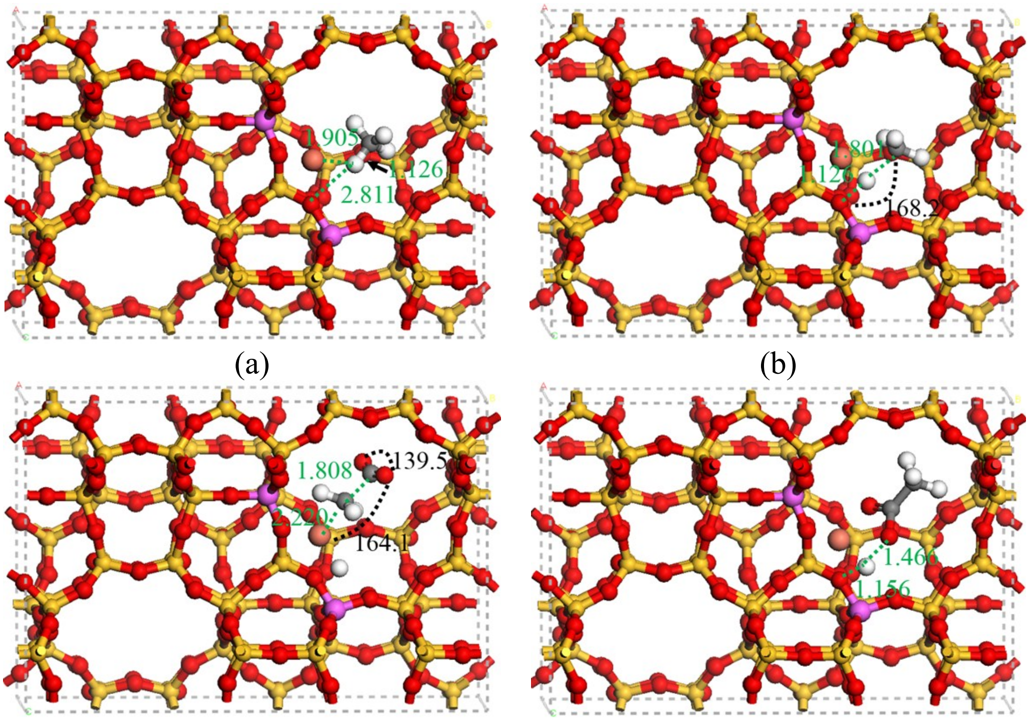

(a) (b)

(c) (d)

Fig. S6. Optimized structure and corresponding structure parameters for CH_4 adsorption (a), CH_4 dissociation (b), C–C coupling (c), and acetate intermediate protonation (d) over MFI zeolite carrying $[Cu]^{2+}$. Atomic coloring: Si, yellow; O, red; Al, pink; Cu, brown; C, grey, and H, white. The units of bond distance and bond angle are Å and degree, respectively.

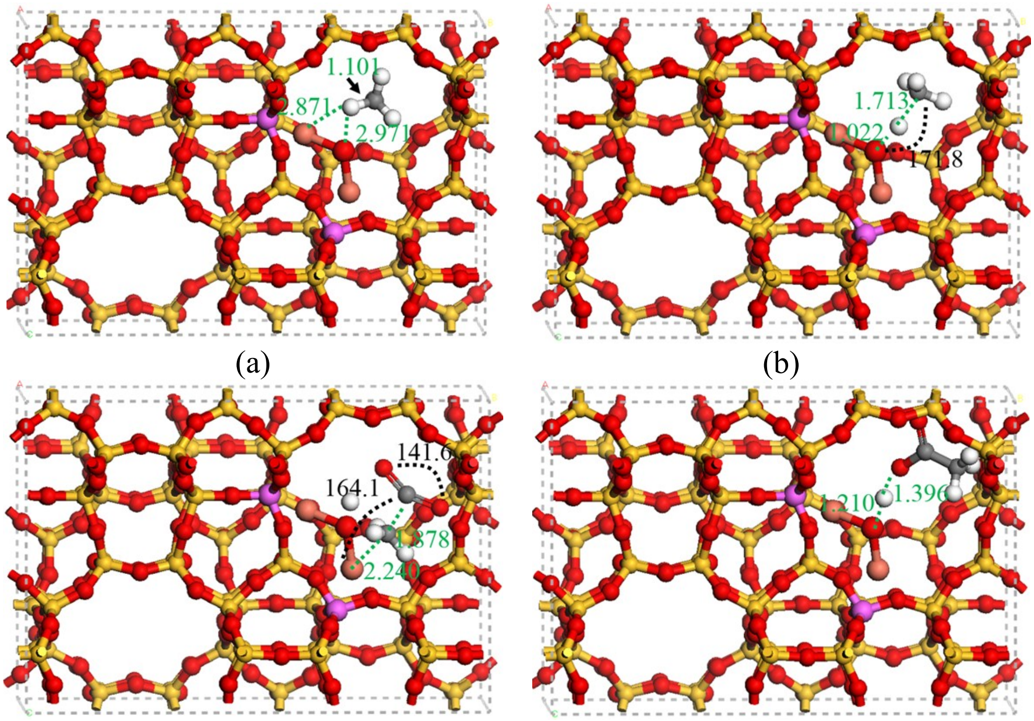

(a) (b)

(c) (d)

Fig. S7. Optimized structure and corresponding structure parameters for CH_4 adsorption (a), CH_4 dissociation (b), C–C coupling (c), and acetate intermediate protonation (d) over MFI zeolite carrying $[CuOCu]^{2+}$. Atomic coloring: Si, yellow; O, red; Al, pink; Cu, brown; C, grey, and H, white. The units of bond distance and bond angle are Å and degree, respectively.

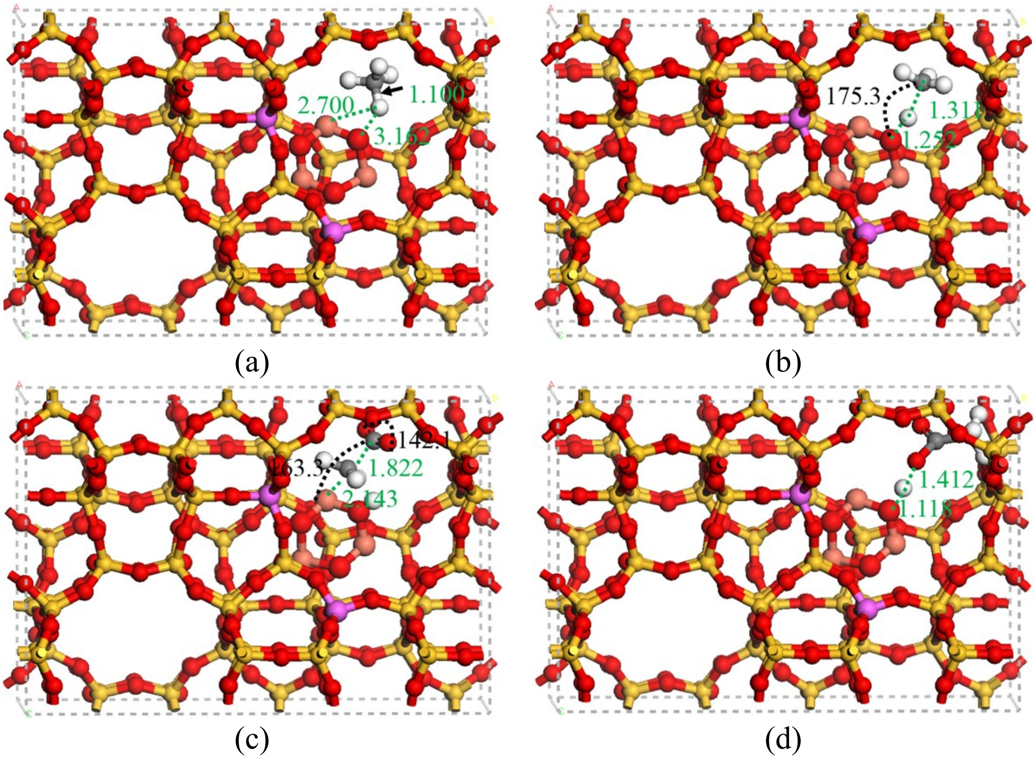

(a) (b)

(c) (d)

Fig. S8. Optimized structure and corresponding structure parameters for CH_4 adsorption (a), CH_4 dissociation (b), C–C coupling (c), and acetate intermediate protonation (d) over MFI zeolite carrying $[Cu_3(\mu\text{-}O)_3]^{2+}$. Atomic coloring: Si, yellow; O, red; Al, pink; Cu, brown; C, grey, and H, white. The units of bond distance and bond angle are Å and degree, respectively.

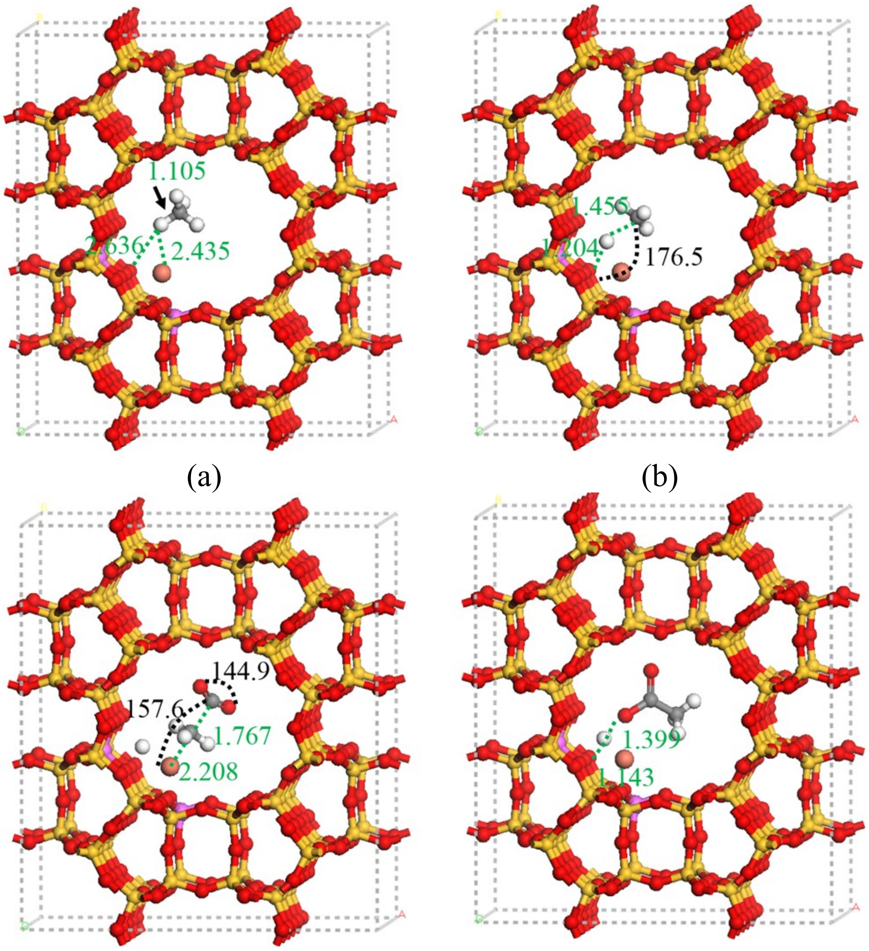

(a) (b)

(c) (d)

Fig. S9. Optimized structure and corresponding structure parameters for CH_4 adsorption (a), CH_4 dissociation (b), C–C coupling (c), and acetate intermediate protonation (d) over MOR zeolite carrying $[Cu]^{2+}$. Atomic coloring: Si, yellow; O, red; Al, pink; Cu, brown; C, grey, and H, white. The units of bond distance and bond angle are Å and degree, respectively.

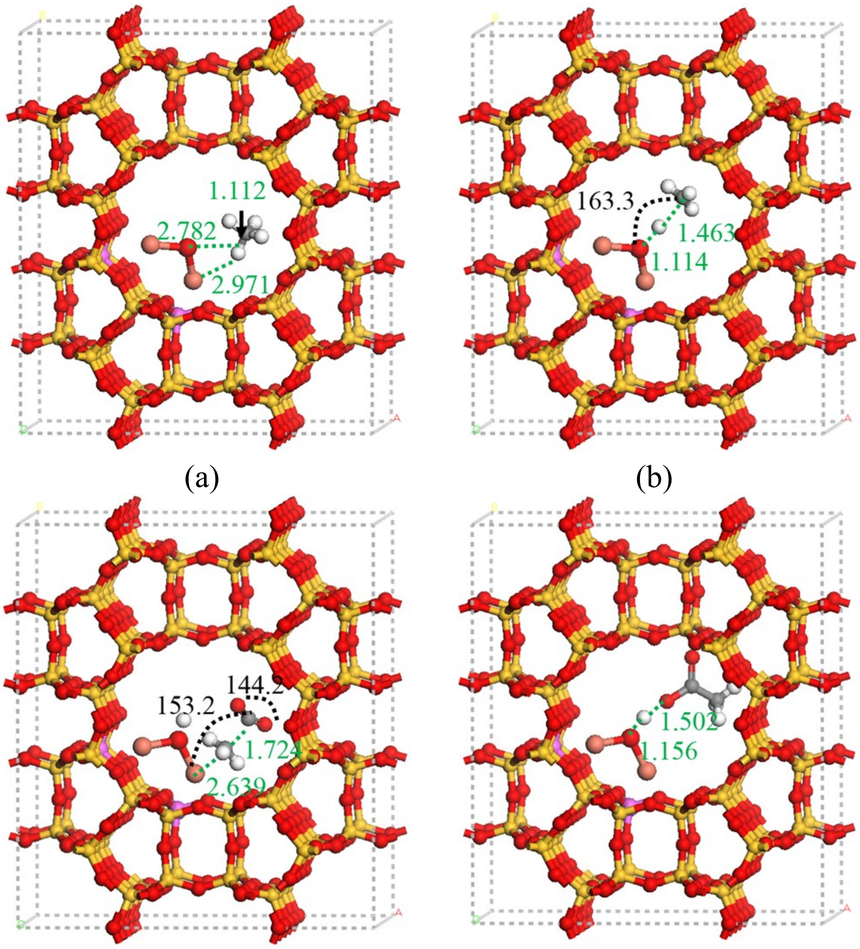

(a) (b)

(c) (d)

Fig. S10. Optimized structure and corresponding structure parameters for CH_4 adsorption (a), CH_4 dissociation (b), C–C coupling (c), and acetate intermediate protonation (d) over MOR zeolite carrying $[CuOCu]^{2+}$. Atomic coloring: Si, yellow; O, red; Al, pink; Cu, brown; C, grey, and H, white. The units of bond distance and bond angle are Å and degree, respectively.

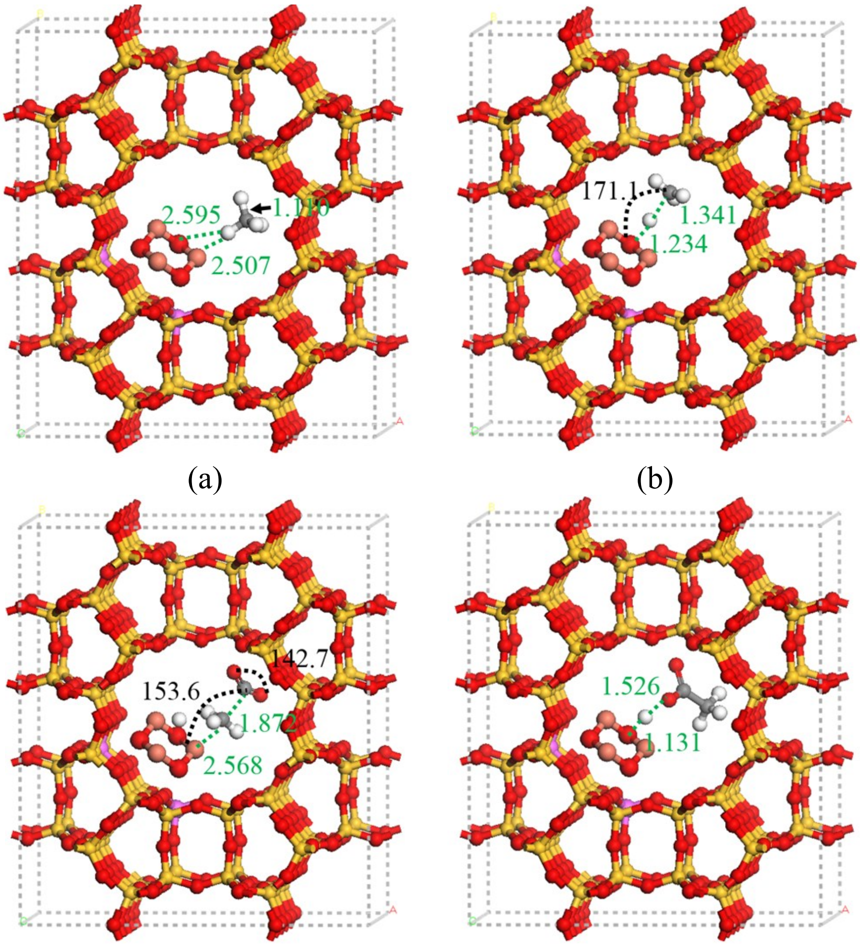

(a) (b)

(c) (d)

Fig. S11. Optimized structure and corresponding structure parameters for CH_4 adsorption (a), CH_4 dissociation (b), C–C coupling (c), and acetate intermediate protonation (d) over MOR zeolite carrying $[Cu_3(\mu\text{-}O)_3]^{2+}$. Atomic coloring: Si, yellow; O, red; Al, pink; Cu, brown; C, grey, and H, white. The units of bond distance and bond angle are Å and degree, respectively.

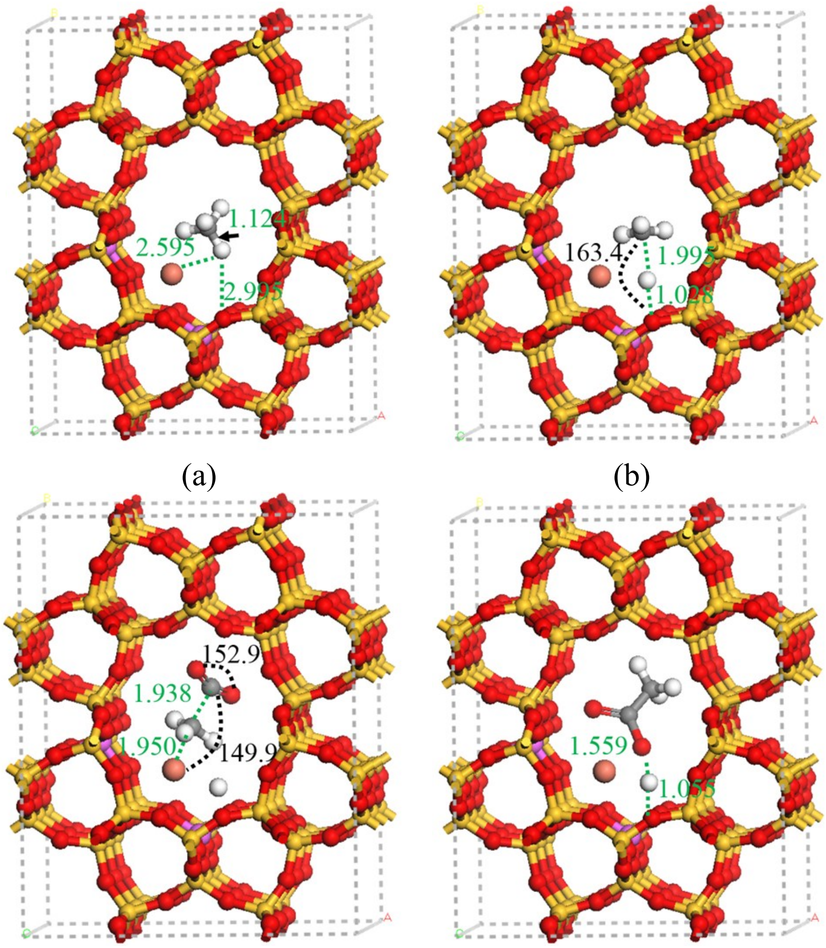

(a) (b)

(c) (d)

Fig. S12. Optimized structure and corresponding structure parameters for CH_4 adsorption (a), CH_4 dissociation (b), C–C coupling (c), and acetate intermediate protonation (d) over TON zeolite carrying $[Cu]^{2+}$. Atomic coloring: Si, yellow; O, red; Al, pink; Cu, brown; C, grey, and H, white. The units of bond distance and bond angle are Å and degree, respectively.

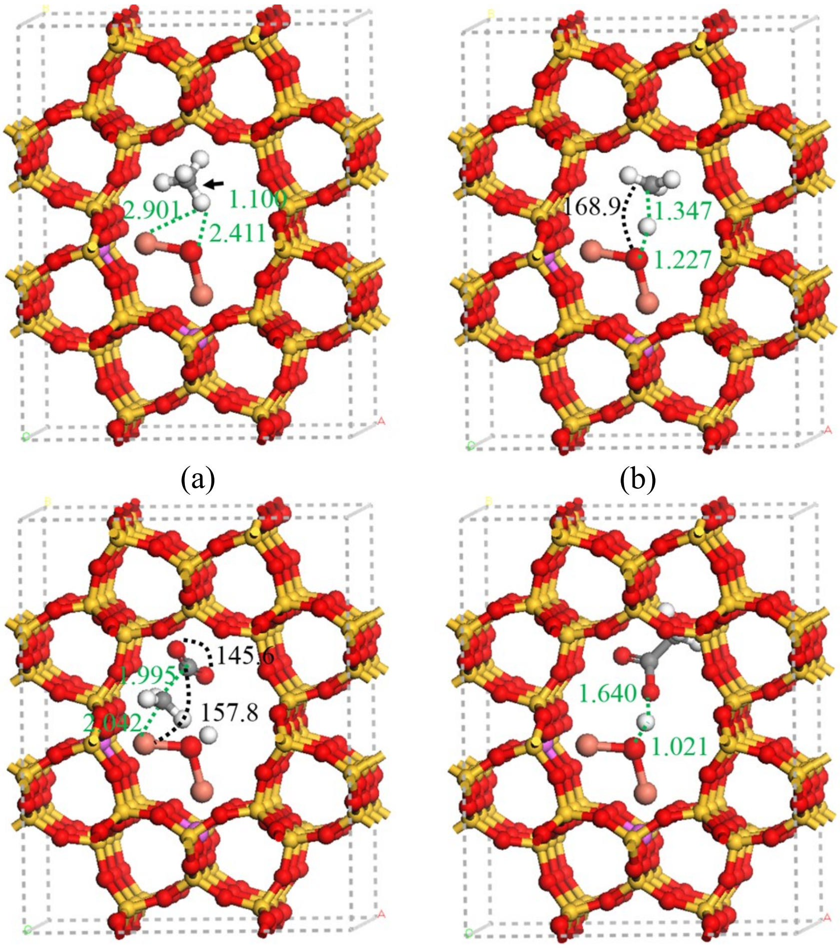

(a) (b)

(c) (d)

Fig. S13. Optimized structure and corresponding structure parameters for CH_4 adsorption (a), CH_4 dissociation (b), C–C coupling (c), and acetate intermediate protonation (d) over TON zeolite carrying $[CuOCu]^{2+}$. Atomic coloring: Si, yellow; O, red; Al, pink; Cu, brown; C, grey, and H, white. The units of bond distance and bond angle are Å and degree, respectively.

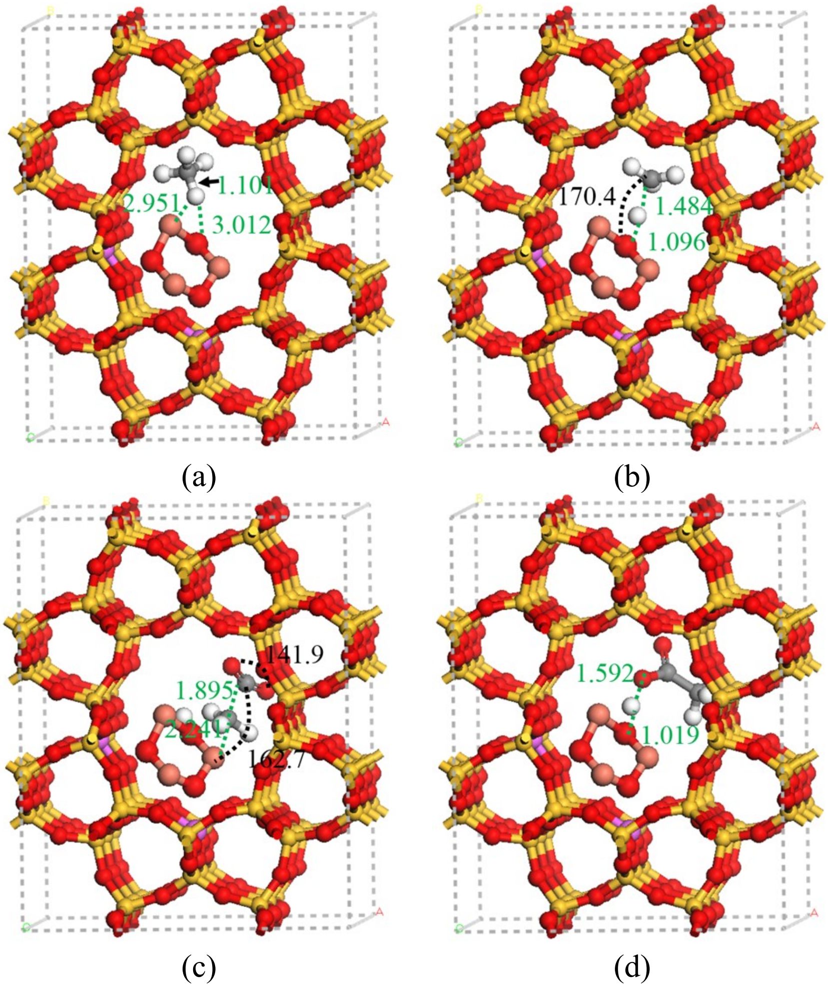

(a) (b)

(c) (d)

Fig. S14. Optimized structure and corresponding structure parameters for CH_4 adsorption (a), CH_4 dissociation (b), C–C coupling (c), and acetate intermediate protonation (d) over TON zeolite carrying $[Cu_3(\mu\text{-}O)_3]^{2+}$. Atomic coloring: Si, yellow; O, red; Al, pink; Cu, brown; C, grey, and H, white. The units of bond distance and bond angle are Å and degree, respectively.

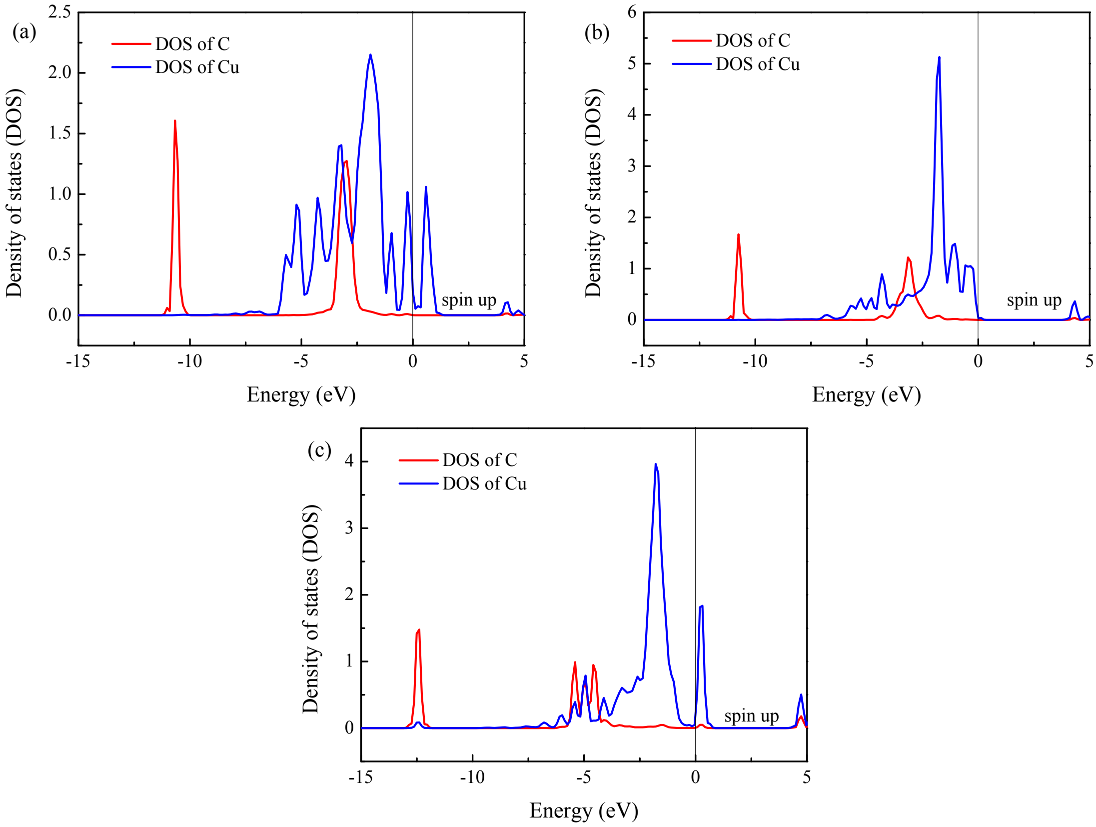

Fig. S15. Density of states (DOS) of the s, p orbital of C atom in CH_4 and the s, p, d orbital of Cu atom in $[Cu]^{2+}$ (a), $[CuOCu]^{2+}$ (b), and $[Cu_3(\mu\text{-}O)_3]^{2+}$ (c) for CH_4 adsorption on the MFI zeolite. The solid line is the Fermi level.

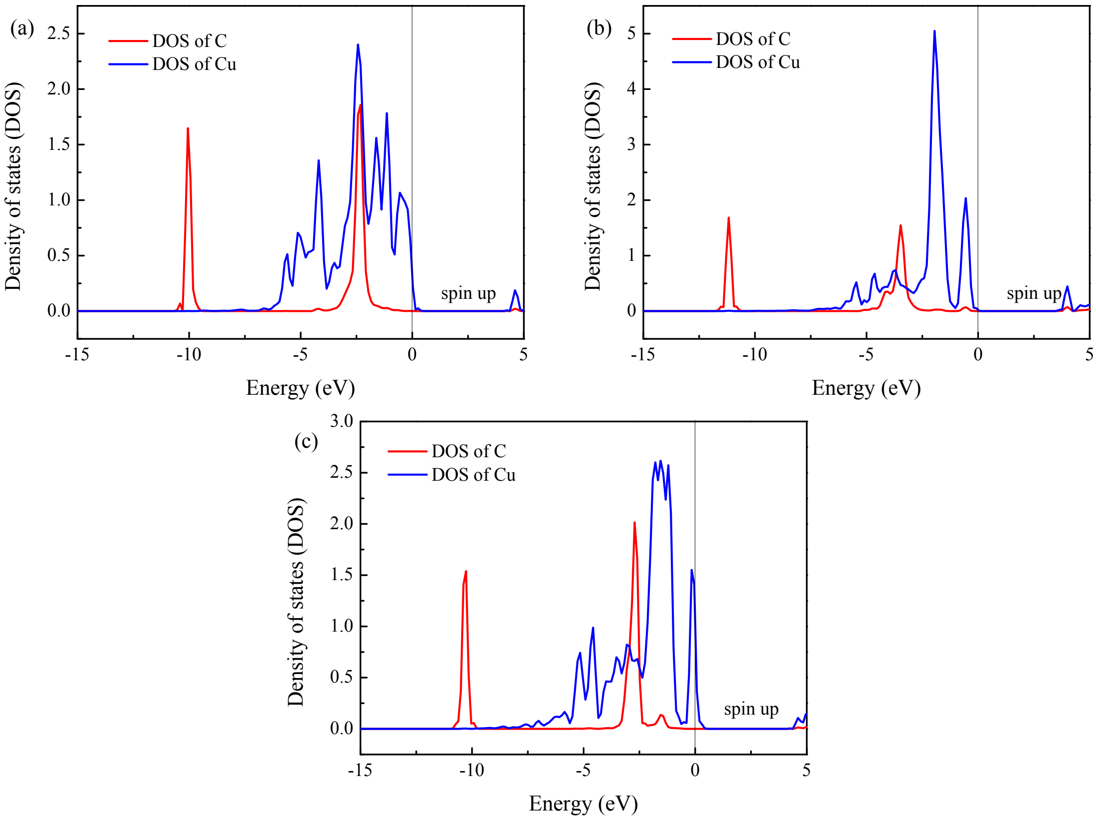

Fig. S16. Density of states (DOS) of the s, p orbital of C atom in CH_4 and the s, p, d orbital of Cu atom in $[Cu]^{2+}$ (a), $[CuOCu]^{2+}$ (b), and $[Cu_3(\mu\text{-}O)_3]^{2+}$ (c) for CH_4 adsorption on the MOR zeolite. The solid line is the Fermi level.

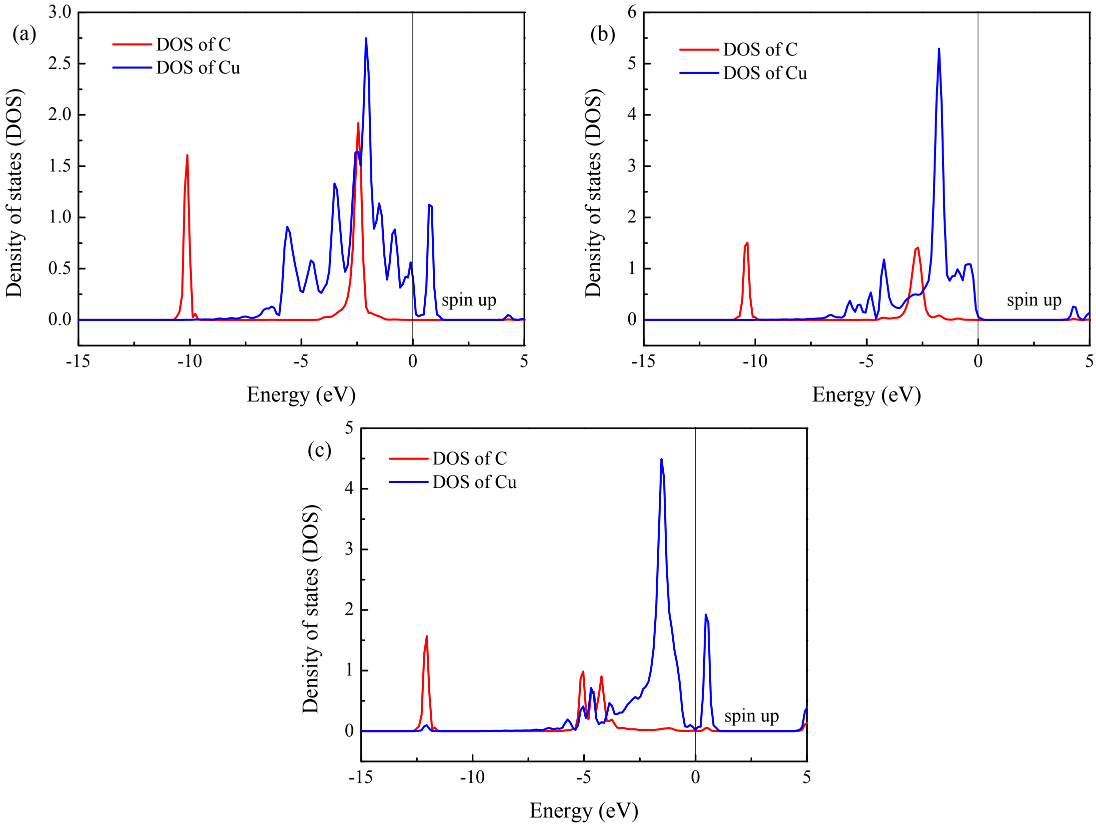

Fig. S17. Density of states (DOS) of the s, p orbital of C atom in CH_4 and the s, p, d orbital of Cu atom in $[Cu]^{2+}$ (a), $[CuOCu]^{2+}$ (b), and $[Cu_3(\mu\text{-}O)_3]^{2+}$ (c) for CH_4 adsorption on the TON zeolite. The solid line is the Fermi level.

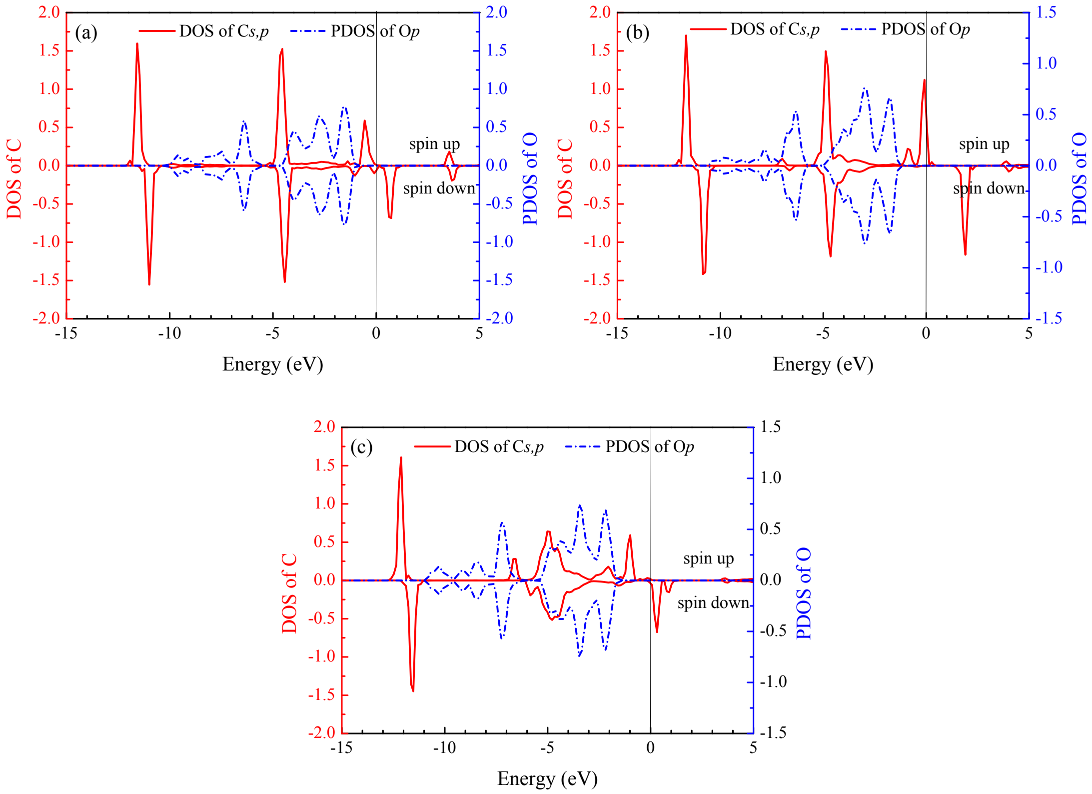

Fig. S18. Projected density of states (PDOS) for the s, p orbital of C atom in $–CH_3$ and the p orbital of O atom in the transition state of CH_4 dissociation over MFI zeolite carrying $[Cu]^{2+}$ (a), $[CuOCu]^{2+}$ (b), and $[Cu_3(\mu\text{-}O)_3]^{2+}$ (c). The solid line is the Fermi level.

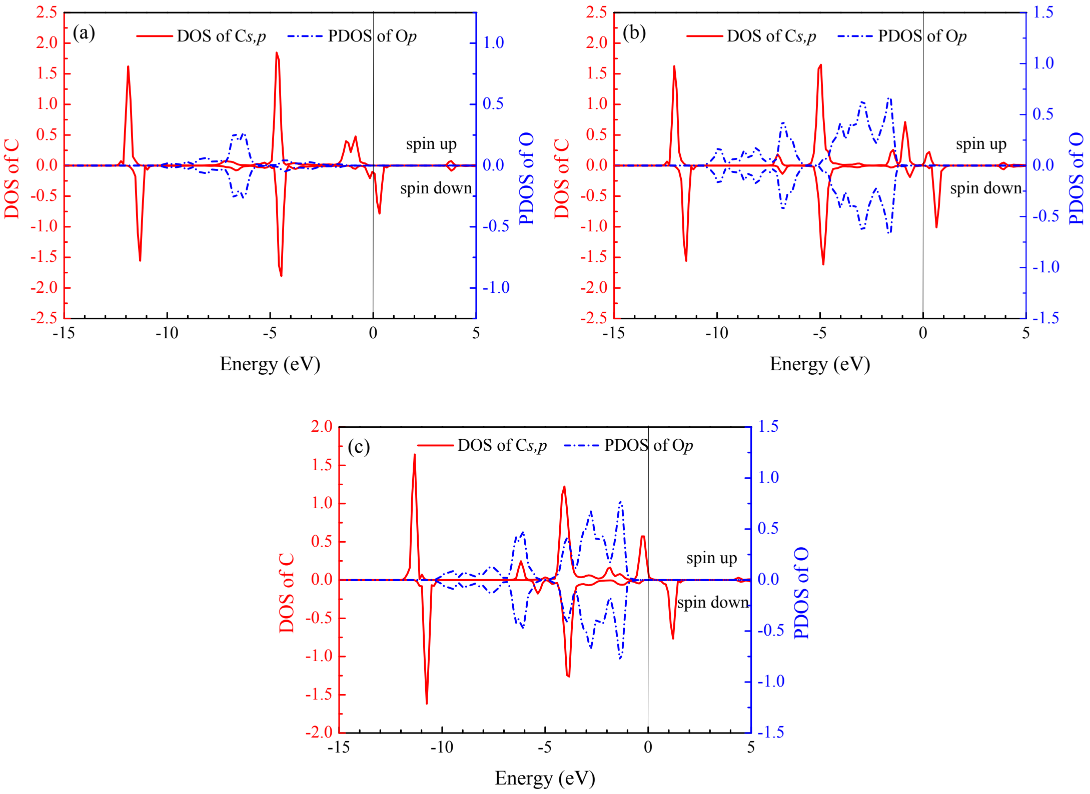

Fig. S19. Projected density of states (PDOS) for the s, p orbital of C atom in –CH_3 and the p orbital of O atom in the transition state of CH_4 dissociation over MOR zeolite carrying $[Cu]^{2+}$ (a), $[CuOCu]^{2+}$ (b), and $[Cu_3(\mu\text{-}O)_3]^{2+}$ (c) cluster. The solid line is the Fermi level.

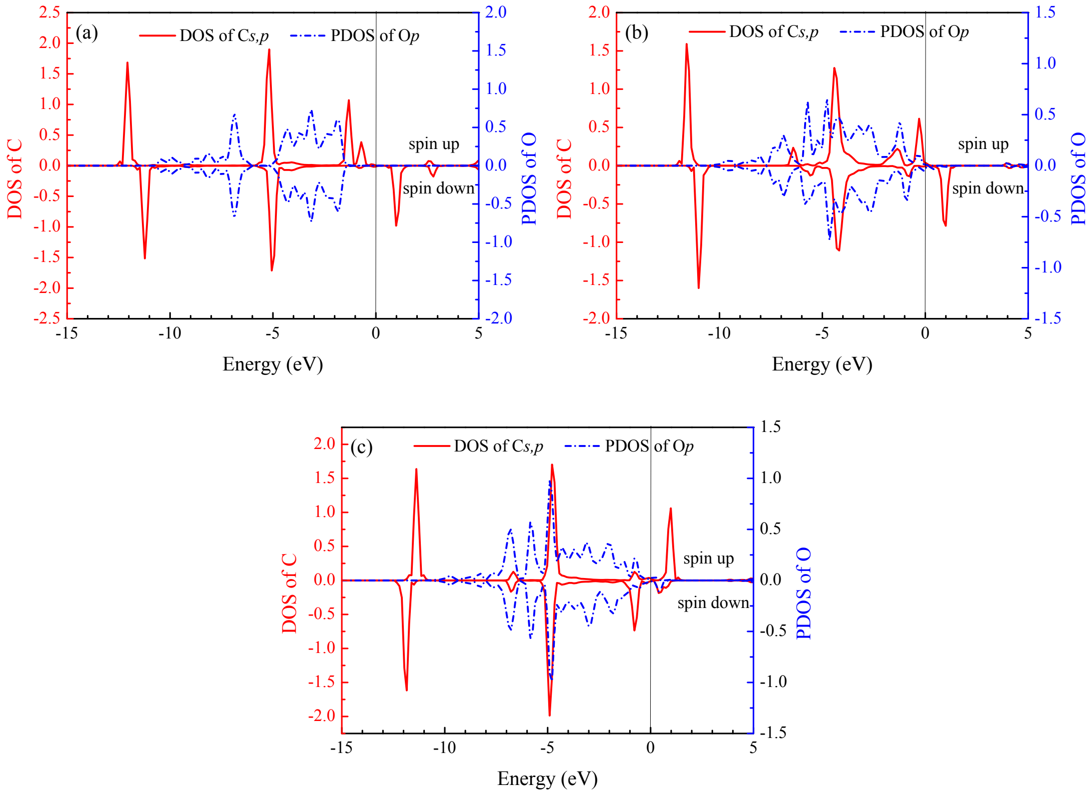

Fig. S20. Projected density of states (PDOS) for the s, p orbital of C atom of –CH_3 and the p orbital of O atom for the transition state of CH_4 dissociation over TON zeolite with $[Cu]^{2+}$ (a), $[CuOCu]^{2+}$ (b), and $[Cu_3(\mu\text{-}O)_3]^{2+}$ (c) cluster. The solid line is the Fermi level.

References:

[1] J. B. Higgins, R. B. LaPierre, J. L. Schlenker, A. C. Rohrman, J. D. Wood, G. T. Kerr and W. J. Rohrbaugh. The Framework Topology of Zeolite-Beta. *Zeolites*. 1988, **8**, 446−452.

[2] D. H. Olson, G. T. Kokotailo, S. L. Lawton and W. M. Meier. Crystal-Structure and Structure-Related Properties of MFI. *J. Phys. Chem*. 1981, **85**, 2238−2243.

[3] Database of Zeolite Structures. http://www.iza-structure.org/databases/.

[4] B. Marler. Silica-TON Synthesis and Singel-Crystal Structure Refinement. *Zeolites*. 1987, **7**, 393−397.